

COSMIC RAY ACCELERATION AT ULTRARELATIVISTIC SHOCK WAVES: EFFECTS OF DOWNSTREAM SHORT-WAVE TURBULENCE

JACEK NIEMIEC

Department of Physics and Astronomy, Iowa State University, Ames, IA 50011 and
 Instytut Fizyki Jądrowej PAN, ul. Radzikowskiego 152, 31-342 Kraków, Poland

MICHał OSTROWSKI

Obserwatorium Astronomiczne, Uniwersytet Jagielloński, ul. Orla 171, 30-244 Kraków, Poland

AND

MARTIN POHL

Department of Physics and Astronomy, Iowa State University, Ames, IA 50011

Draft version July 9, 2018

ABSTRACT

The present paper is the last of a series studying the first-order Fermi acceleration processes at relativistic shock waves with the method of Monte Carlo simulations applied to shocks propagating in realistically modeled turbulent magnetic fields. The model of the background magnetic field structure of Niemiec & Ostrowski (2004, 2006) has been augmented here by a large-amplitude short-wave downstream component, imitating that generated by plasma instabilities at the shock front. Following Niemiec & Ostrowski (2006), we have considered ultrarelativistic shocks with the mean magnetic field oriented both oblique and parallel to the shock normal. For both cases simulations have been performed for different choices of magnetic field perturbations, represented by various wave power spectra within a wide wavevector range. The results show that the introduction of the short-wave component downstream of the shock is not sufficient to produce power-law particle spectra with the “universal” spectral index 4.2. On the contrary, concave spectra with cutoffs are preferentially formed, the curvature and cutoff energy being dependent on the properties of turbulence. Our results suggest that the electromagnetic emission observed from astrophysical sites with relativistic jets, e.g. active galactic nuclei and gamma-ray bursts, is likely generated by particles accelerated in processes other than the widely invoked first-order Fermi mechanism.

Subject headings: acceleration of particles, cosmic rays, gamma rays: bursts, methods: numerical, relativity, shock waves

1. INTRODUCTION

Realistic modeling of first-order Fermi cosmic-ray acceleration at relativistic shock waves is a difficult task due to the strong dependence of the resulting particle spectra on the essentially unknown local conditions at such shocks. Therefore, progress in this field mostly arises from the increasingly more realistic MHD conditions that are assumed to apply near the shocks. For mildly relativistic shocks in the *test particle* approach the advances that have been made in the past twenty years involve a semianalytic solution of the particle pitch-angle diffusion equation at parallel shocks (Kirk & Schneider 1987), the effects of different shock compressions in parallel shocks (Heavens & Drury 1988), the impact of an oblique mean magnetic field for subluminal configurations (Kirk & Heavens 1989), and the effects of oblique field configurations at sub- and superluminal shocks considered with an increasing degree of complication, applying successively more realistic physical approximations (Ostrowski 1991, 1993; Bednarz & Ostrowski 1996; Niemiec & Ostrowski 2004). For ultrarelativistic shocks the notion of a “universal” spectral index was first described by Bednarz & Ostrowski (1998) and later found in a va-

riety of studies (Gallant & Achterberg 1999; Kirk et al. 2000; Achterberg et al. 2001; Lemoine & Pelletier 2003; Ellison & Double 2004), but more recent studies (Niemiec & Ostrowski 2006) indicate basic problems with first-order Fermi acceleration, in particular in generating wide-energy power-law spectra. The latter work also contains a more systematic discussion of the subject literature.

On the other hand, there have been attempts to self-consistently derive the electromagnetic shock structure. One very simplified approach applied modeling of nonlinear effects in the first-order Fermi acceleration at the shock (e.g., Ellison & Double 2002). The limitations of this technique arise from the approximate treatment of particle scattering near the shock and its simple scaling with particle energy instead of a realistic accounting for the microphysics of the process. A more realistic microscopic and self-consistent description of the collisionless shock transition may be afforded by Particle-In-Cell (PIC) simulations (e.g., Hoshino et al. 1992; Silva et al. 2003; Nishikawa et al. 2003, 2005a; Frederiksen et al. 2004; Hededal & Nishikawa 2005; Jaroschek et al. 2005), which follow the formation of a relativistic collisionless shock starting with processes acting on the plasma scale. In these simulations one typically observes that the generation of magnetic and electric fields is accompanied by

an evolution of the particle distribution function from the background plasma conditions up to highly superthermal energy scales. Although providing a wealth of information on the collisionless shock structure, the PIC simulations are still very much limited in dynamical range, in particular for cosmic-ray particles whose energies are many orders of magnitude larger than the plasma particle energies.

The present paper is a continuation of the studies of Niemiec & Ostrowski (2004, 2006). Here we attempt to incorporate the results of the PIC simulations concerning the generation of magnetic fields at relativistic shocks into the test particle Monte Carlo simulations of cosmic-ray particle acceleration. As in the previous papers, we study ultrarelativistic shock waves propagating in a medium with a magnetic field that is perturbed over a wide range of macroscopic scales. However, we also consider an additional short-wave isotropic turbulent field component downstream of the shock, analogous to the shock generated turbulent fields revealed by the PIC simulations. We treat the amplitude of the short-wave component as a model parameter and study the effects of the small-scale perturbations on the particle spectra and angular distributions derived in the previous work.

In what follows, $c = 1$ is the speed of light. The integration of particle trajectories is performed in the respective local plasma (upstream or downstream) rest frame, and we use index “1” (“2”) to label quantities provided in the upstream (downstream) frame. We consider ultrarelativistic particles with $p = E$. We use dimensionless variables, so a particle of unit energy moving in an uniform mean upstream magnetic field \mathbf{B}_0 has the unit maximum (for $p_\perp = E$) gyroradius $r_g(E = 1) = 1$ and the respective resonance wavevector is $k_{res}(E = 1) = 2\pi$.

2. DETAILS OF THE MODELING

2.1. Magnetic Field Structure

As in Niemiec & Ostrowski (2004, 2006) we assume a relativistic shock wave to propagate with velocity \mathbf{u}_1 (or the respective Lorentz factor γ_1) in the upstream medium with a uniform magnetic field $\mathbf{B}_0 \equiv \mathbf{B}_{0,1}$, inclined at an angle ψ_1 to the shock normal (along \mathbf{u}_1 direction), superimposed on which are isotropic 3D magnetic field perturbations. These perturbations are characterized with a power-law wave power spectrum $F(k) \sim k^{-q}$ that is defined in a wide wavevector range $(k_{1,min}, k_{1,max})$, where $k_{1,min} = 0.0001$ and $k_{1,max} = 10$. Specifically we consider the wave spectral indices $q = 1$, describing the flat power spectrum, and $q = 5/3$ for the Kolmogorov distribution. The integral power of these perturbations is given by the (upstream) amplitude

$$\delta B = \sqrt{\int_{k_{1,min}}^{k_{1,max}} F(k) dk}, \quad (1)$$

and $\delta B/B_0$ is one of our model parameters. As described in detail in Niemiec & Ostrowski (2004, 2006), the upstream field perturbations are modeled as the superposition of static sinusoidal waves of finite amplitude. The downstream magnetic field structure, including the turbulent component, is derived as the shock-compressed upstream field, and hence the downstream turbulent magnetic field is naturally anisotropic. Our method of applying the hydrodynamical shock jump conditions (for

the electron-proton plasma, Heavens & Drury 1988) preserves the continuity of the magnetic field lines across the shock. In what follows, we refer to the field component described above as the *large-scale* (or *long-wave*) *background field*.

The other physical magnetic field component considered in the present study is the short-wave turbulence, assumed to be a result of kinetic magnetic field generation processes acting at the shock. This component, taken for simplicity to be isotropic¹ and static, is imposed upon the nonuniform background magnetic field downstream of the shock. The short-wave nonlinear field perturbations are introduced with a flat spectral distribution in the wavevector range $(10k_{2,max}, 100k_{2,max})$, where the shortest downstream waves are the shock-compressed shortest upstream waves:

$$k_{2,max} = k_{1,max} R \frac{\gamma_1}{\gamma_2}. \quad (2)$$

Here $R = u_1/u_2$ is the compression ratio in the shock rest frame, and γ_1 (γ_2) is the upstream (downstream) shock Lorentz factor. The wavevector range of the small-scale turbulent component is chosen to be one decade in k apart from $k_{2,max}$ to separate the influence of these perturbations on the low-energy particle motion from that exerted by the short-wave component of the large-scale background field. This choice also facilitates the use of a hybrid method for the calculation of particle trajectories (see §2.2). Note also, that the definition of the short-wave component depends on the Lorentz factor of the shock. Below, we refer to the short-wave magnetic field component also as the *shock-generated turbulence* (“sh”), to distinguish it from the large-scale background field, that exists in the upstream region and is only compressed upon passage through the shock.

In our simulations we exclusively study the first-order Fermi acceleration process and neglect second-order processes. Therefore, the turbulent magnetic field components (both short-wave and large-scale background perturbations) can be considered to be static in the respective plasma rest frames, both upstream and downstream of the shock, and electric fields that may exist in the shock transition layer are neglected.

2.2. Monte Carlo Simulations

The implementation of short-wave turbulence into the Monte Carlo simulations forces us to dispense with the direct integration of the particle equations of motion in the analytically modeled magnetic field (see Niemiec & Ostrowski 2006). Instead, we resume the derivation of particle trajectories with the hybrid approach proposed in Niemiec & Ostrowski (2004). Thus, particle trajectories are directly calculated from the equations of motion in the large-scale background magnetic field only, whereas the trajectory perturbations due

¹ Theoretical considerations by Medvedev & Loeb (1999) and numerical PIC simulations (e.g., Silva et al. 2003; Nishikawa et al. 2003; Frederiksen et al. 2004) show that the relativistic two-stream (Weibel-like) instability at the relativistic collisionless shock front leads to the generation of a strong, small-scale turbulent field downstream, that is predominantly transversal (2D) and lies in the plane of the shock. Because the magnetic field in the nonlinear regime of the two-stream instability is sustained by the structure of the ion current channels, instabilities in the ion filaments (e.g., kink and/or firehose instability) should lead ultimately to the 3D turbulent magnetic field.

to the shock-generated small-scale turbulence are accounted for through a small-amplitude pitch-angle scattering term. Auxiliary simulations have been performed to determine the scattering amplitude distributions for various particle energies. In the scattering procedure, after each time step Δt the particle momentum direction is perturbed by a small angle $\Delta\Omega$. The time step itself scales with particle energy (or gyroradius), $\Delta t \propto E$, and is chosen so that the condition $c\Delta t \gg \lambda_{sh}$ is always fulfilled (λ_{sh} is the wavelength of shock-generated perturbations), which means that the auxiliary simulations follow the particle scattering on the shock-generated turbulence well into the diffusive regime. Therefore, the scattering amplitude distributions also scale linearly with the short-wave turbulence amplitude, and the mean scattering angle variations are related to the particle energy as $\Delta\Omega \propto E^{-1/2}$.

An individual simulation run is performed as follows. We start with injecting monoenergetic particles (with the initial energy $E_0 = 0.1$) at random positions along the shock front, with their momenta isotropically distributed within a cone around the shock normal pointing upstream of the shock. In an initial simulation cycle, the injection process is continued until the required number of particles, N , has been selected—those that after being injected upstream and then transmitted downstream of the shock, succeed in recrossing the shock front again. Then the calculation of individual particle trajectories proceeds through all subsequent upstream-downstream cycles. In each cycle, a fraction of the particles escapes through a free-escape boundary introduced “far downstream” of the shock, i.e. at a location from which there is only a negligible chance that particles crossing the boundary would return back to the shock. To the particles remaining in the simulations the trajectory-splitting procedure is applied (see Niemiec & Ostrowski 2004), so the number of particles remains constant in the acceleration process, but the statistical weights of the particles are appropriately reduced. The final spectra and angular distributions of accelerated particles, derived in the shock normal rest frame for particles crossing the shock front, are averaged over many statistically different simulation runs.

3. RESULTS

Because of the limited capabilities of present-day computers, the long-time nonlinear development of plasma instabilities leading to the generation of the short-wave turbulent downstream magnetic field component cannot yet be fully investigated, in particular for electron-ion plasma collision fronts. Therefore, the ultimate structure of the small-scale field and the global effectiveness of the generation mechanism remain uncertain. To estimate the role of the shock-generated turbulence in cosmic-ray acceleration at ultrarelativistic shocks, we introduce the small-scale wave component as isotropic 3D magnetic field perturbations and treat the amplitude of these perturbations as a model parameter.

The spectra of accelerated particles for oblique superluminal shocks are presented in Figures 1-4, and those for parallel shocks are displayed in Figures 6 and 8. The amplitude of the short-wave component, $\delta B_{sh}/\langle B_2 \rangle$, as provided in the figures, is measured in units of the average downstream perturbed magnetic field strength

$\langle B_2 \rangle = \langle (\mathbf{B}_{0,2} + \delta \mathbf{B}_2)^2 \rangle^{1/2}$. The spectra presented with solid lines has been derived in the turbulence model without the δB_{sh} term (most of them are presented in Niemiec & Ostrowski 2006). Some of the energetic particle distributions follow a power-law in a certain energy range. In these cases linear fits to the power-law portions of the spectra are presented, and values of the phase-space spectral indices, α , are given (the equivalent *number* spectral index $\sigma = \alpha - 2$). The spectral indices may help to make a quantitative comparison of the spectra, but care must be exercised, because the spectral indices depend on the energy range chosen for the fit on account of the curvature in most of the spectra. In the case of superluminal shocks, we use the same low-energy limit for the energy range selected for the fits.

3.1. Oblique Superluminal Shocks

Accelerated particle spectra for oblique superluminal shocks are presented in Figures 1-3 for $\psi_1 = 45^\circ$ ($u_1/\cos\psi_1 \approx 1.4c$), and in Figure 4 for $\psi_1 = 90^\circ$ (perpendicular shock). One can see that increasing the amplitude of the shock-generated turbulence leads to a more efficient acceleration with particle spectral tails extending to higher energies. However, in all cases, in which $\delta B_{sh}/\langle B_2 \rangle \gg 1$, the energetic spectral tails are convex, so the spectral index increases with particle energy. In addition, all the spectra have cutoffs at an energy for which the resonance condition for interactions with the long-wave turbulence is fulfilled. These features result from the fact that the influence on particle trajectories of the shock-generated small-scale turbulence decreases with increasing particle energy. In our numerical approach this corresponds to a reduction of the scattering amplitude $\Delta\Omega(E)$ (see §2.2).

Most published treatments of first-order Fermi acceleration at ultrarelativistic shocks, that apply the pitch-angle diffusion approximation (Bednarz & Ostrowski 1998; Gallant & Achterberg 1999; Kirk et al. 2000; Achterberg et al. 2001; Ellison & Double 2004; Keshet & Waxman 2005), assume scattering conditions that do not change with particle energy. As discussed by Ostrowski & Bednarz (2002), these authors show that if the small-angle scattering dominates over the possible influence of the oblique mean magnetic field component and/or the long-wave perturbations in shaping the particle trajectories, then power-law particle distributions with “universal” spectral index $\alpha_u \approx 4.2$ may be formed. With the more realistic magnetic field model considered in the present paper, it is not possible to reproduce these results. However, particle spectra can approach a power-law form in a limited energy range near the particle injection energy, as demonstrated by the fits to the low-energy parts of the spectra in Figures 1-4. The energy ranges for the fits are arbitrary selected but have the same low-energy bound. Note that in the figures the spectral indices, though depending on the background conditions, are *always* larger than α_u . If one chose higher energies to derive a power-law fit to the spectra, one would obtain a higher spectral index on account of the convex shapes of the spectra. Convex spectra could have been expected based on the earlier studies of Bednarz & Ostrowski (1998), who showed how an increased pitch-angle scattering angle in superluminal shocks leads to a flattening of the particle

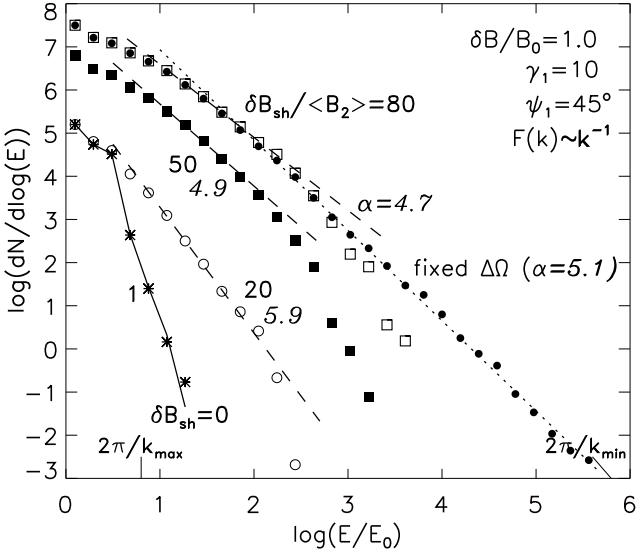


FIG. 1.— Accelerated particle spectra at oblique superluminal shocks with $\gamma_1 = 10$, $\psi_1 = 45^\circ$, and a flat wave-power spectrum of large-scale background magnetic field turbulence. The amplitude of the upstream field perturbations is $\delta B/B_0 = 1.0$. The amplitudes of the downstream shock-generated turbulence, $\delta B_{sh}/\langle B_2 \rangle$, are given near the respective spectra. Linear fits to some spectra are also presented with dashed lines. The energy ranges selected for the fits have the same low-energy bounds to facilitate comparison of the spectral indices α , given in italic. The spectrum plotted with a solid line applies to the case without short-wave shock-generated perturbations. The spectrum shown with filled dots is calculated with a fixed scattering term for $E \geq 16$, and the linear fit to the part of this spectrum above $E \geq 16$ is presented with dotted line. Some spectra are vertically shifted for clarity. Particles in the energy range $(2\pi/k_{max}, 2\pi/k_{min})$ can satisfy the resonance condition $k_{res} = 2\pi/r_g(E)$ for some of the waves in the background turbulence spectrum.

spectrum to the limiting “universal” power law (see the discussion of this effect in Ostrowski & Bednarz 2002). To further illustrate this behavior, we have recalculated the spectrum for $\delta B_{sh}/\langle B_2 \rangle = 80$ in Figure 1 (filled dots) for a fixed scattering amplitude $\Delta\Omega(E)$ at particle energies $E \geq 16$ ($\Delta\Omega(E \geq 16) = \text{const.} \ll 1$). Then the pitch-angle scattering term dominates downstream of the shock at high particle energies, which leads to a power-law spectrum formation over a wide energy range without a steepening or a cutoff, but with $\alpha > \alpha_u$.

In the case of superluminal shocks, the particle spectra calculated for a high amplitude of shock-generated turbulence, $\delta B_{sh}/\langle B_2 \rangle = 50$ in Figures 1-4, depend only weakly on the background large-scale magnetic field structure, in contrast to the $\delta B_{sh} = 0$ limit (see also Niemiec & Ostrowski 2006). The acceleration process is only slightly more efficient in the case of a large amplitude of long-wave perturbations ($\delta B/B_0 = 1.0$ in Figs. 1 and 2), in which the spectral tails extend to marginally higher energies and show softer cutoffs, when compared to the cases with $\delta B/B_0 = 0.3$ (Figs. 3 and 4). There are also only minor differences between the spectra derived for a flat spectrum of background perturbations, for which the wave power is uniformly distributed per logarithmic wavevector range, and for the Kolmogorov distribution, for which most power is carried by long waves. In the latter case, one finds power-law particle spectra in a slightly wider energy range than in the case

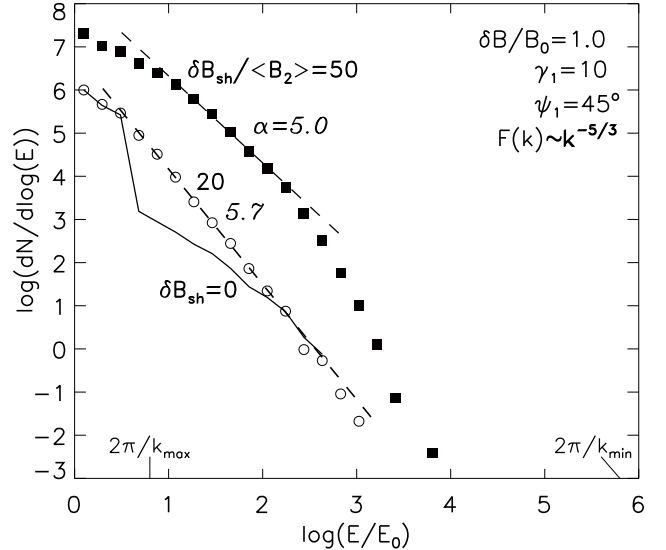


FIG. 2.— Particle spectra derived for oblique superluminal shocks for different amplitudes of shock-generated turbulence. For all spectra $\gamma_1 = 10$, $\psi_1 = 45^\circ$, and a Kolmogorov power spectrum of background long-wave turbulence with $\delta B/B_0 = 1.0$ has been assumed. The spectrum shown with the solid line is derived in the limit $\delta B_{sh} = 0$ (see Fig. 2 in Niemiec & Ostrowski 2006).

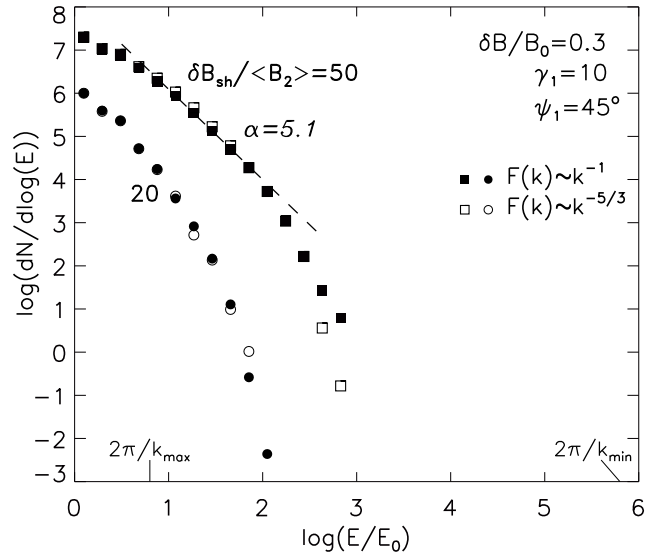


FIG. 3.— Particle spectra at superluminal ($\gamma_1 = 10$, $\psi_1 = 45^\circ$) shocks with $\delta B/B_0 = 0.3$. Filled and open symbols refer to results for a flat and a Kolmogorov wave-power spectrum of large-scale background field perturbations, respectively. The linear fit to the spectrum for the flat wave power spectrum is derived in an energy range with the same low-energy bound as used for the fits shown in Figs. 1 and 2.

of flat distributions (compare Figs. 1 and 2 and spectra in Fig. 4), but the high-energy tails and the cutoff shape remain nearly the same for both types of the wave power spectra.

The structure of the background large-scale magnetic field can, however, influence particle acceleration for smaller amplitudes of the short-wave turbulence. As one can see in Figure 2, the power-law part of the spectrum for $\delta B_{sh}/\langle B_2 \rangle = 20$ and Kolmogorov-type long-wave turbulence spectrum, although steeper, continues

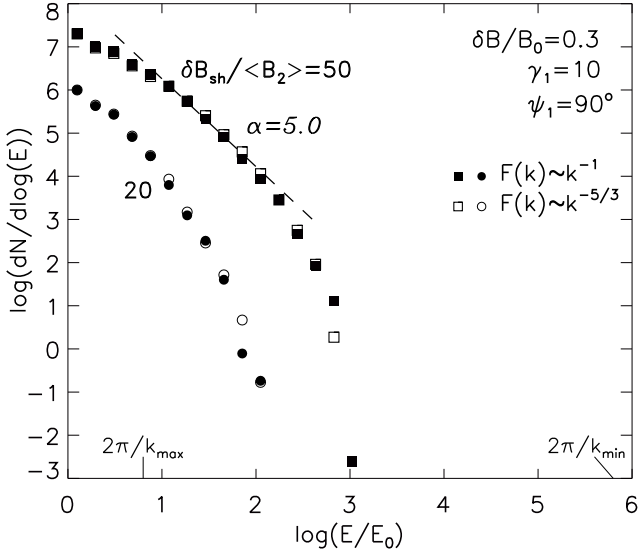


FIG. 4.— Particle spectra at perpendicular ($\gamma_1 = 10$, $\psi_1 = 90^\circ$) shocks for the same parameter combinations as in Fig. 3.

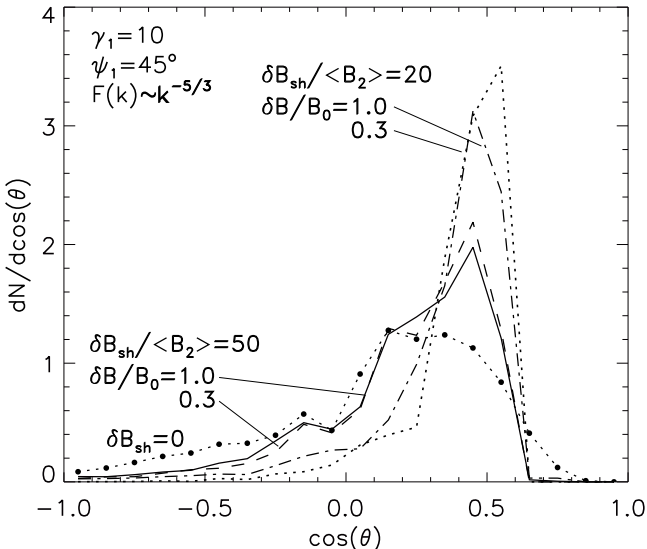


FIG. 5.— Normalized particle angular distributions as measured in the shock rest frame for superluminal shock waves with $\gamma_1 = 10$, $\psi_1 = 45^\circ$, and a Kolmogorov wave power spectrum of large-scale background magnetic field turbulence. Particles with $\cos\theta < 0$ are directed upstream of the shock. The distributions are calculated by summing the quantity $w/(|v_x| + 0.005)$ in the respective $\cos\theta$ -bins at every particle shock crossing, where θ is the angle between the particle momentum and the shock normal, v_x is the normal component of the particle velocity, and w is the statistical weight of the particle. Only particles with $E \geq 1$ are included, and low-energy particles with large weights contribute most to the distributions. The angular distribution presented with filled dots is derived without short-wave perturbations ($\delta B_{sh} = 0$). The distributions for $\delta B_{sh}/\langle B_2 \rangle = 50$, and for $\delta B/B_0 = 1.0$ and 0.3 are presented with solid and dashed lines, respectively. The angular distributions for $\delta B_{sh}/\langle B_2 \rangle = 20$, and $\delta B/B_0 = 1.0$ and 0.3 are shown with dash-dotted and dotted lines, respectively.

to higher energies than that for $\delta B_{sh}/\langle B_2 \rangle = 50$, which is caused by the large-scale component providing particle scattering at higher energies (see, e.g., the spectrum for $\delta B_{sh} = 0$ in Fig. 2). This is not the case for either a flat spectrum (Fig. 1) or a small-amplitude (Fig. 3)

of long-wave turbulence, since in superluminal shocks particle acceleration processes in the absence of large-amplitude long-wave magnetic field perturbations are inefficient (Begelman & Kirk 1990; Niemiec & Ostrowski 2004, 2006).

Figure 5 presents particle angular distributions for superluminal shocks ($\psi_1 = 45^\circ$) with the Kolmogorov power spectrum of large-scale magnetic field perturbations. Note that the angular distributions for a large amplitude of the small-scale turbulence, $\delta B_{sh}/\langle B_2 \rangle = 50$, are closer to that for $\delta B_{sh} = 0$ (filled dots) than angular distributions for the smaller amplitude, $\delta B_{sh}/\langle B_2 \rangle = 20$. As the particle spectra, the distributions for $\delta B_{sh}/\langle B_2 \rangle = 50$ do not depend on the amplitude of the background field perturbations, nor on their wave-power spectrum (distributions for the flat power spectrum are not shown for presentation clarity). Similarity in shape of these distributions to the angular distribution derived without the δB_{sh} scattering term is caused by efficient particle scattering on the downstream short-wave perturbations at low particle energies, which enables a considerable fraction of them to return upstream of the shock. The difference in the distributions for the smaller short-wave amplitude, $\delta B_{sh}/\langle B_2 \rangle = 20$, illustrates the effects the long-wave turbulence has on the particle acceleration process, as discussed above.

A caveat is in order concerning the low-energy part of the simulated spectra. In our simulations with large-amplitude short-wave turbulence, the scattering amplitudes for low particle energies, $E \leq 1$ for the spectra with $\delta B_{sh}/\langle B_2 \rangle = 50$ and $E \leq 5$ for $\delta B_{sh}/\langle B_2 \rangle = 80$, violate the pitch-angle diffusion requirement $\Delta\Omega \ll 1$. This is because in our approach the time between subsequent scatterings is fixed for a given particle energy, and the scattering angle scales linearly with δB_{sh} (see §2.2) providing large scattering amplitudes for large values of $\langle B_2 \rangle$. Therefore, the simulated spectra may suffer a weak systematic flattening at low energies.

3.2. Parallel Shocks

As discussed by Ostrowski & Bednarz (2002), the particle spectra with “universal” slope have been derived in conditions equivalent to a parallel ($\psi_1 = 0^\circ$) mean shock configuration. In our earlier work (Niemiec & Ostrowski 2004, 2006) we have demonstrated that the spectra formed at parallel relativistic shocks depend substantially on background conditions, and features such as a relation between the spectral index and the turbulence amplitude or a cutoff formation in the case of ultrarelativistic shocks can be observed. In this section, we investigate the role of shock-generated downstream turbulence in particle acceleration at parallel shocks. For that purpose, we have performed simulations for highly relativistic shock waves with Lorentz factor $\gamma_1 = 10$ and 30, as presented in Figures 6 and 8, respectively. For parallel shocks the amplitude of the compressed background field downstream of the shock, $\langle B_2 \rangle$, is on average much smaller than for the oblique shocks discussed in §3.1. Therefore, the numerical constraints are largely relaxed, and we can use larger values of $\delta B_{sh}/\langle B_2 \rangle$, up to 300 or even 500. However, we would still slightly violate the pitch-angle scattering approximation at $E \leq 1$ for the spectra with $\delta B_{sh}/\langle B_2 \rangle = 80$ in Figs. 6a and 6b, and $\delta B_{sh}/\langle B_2 \rangle = 300$ in Figs. 6c and 6d.

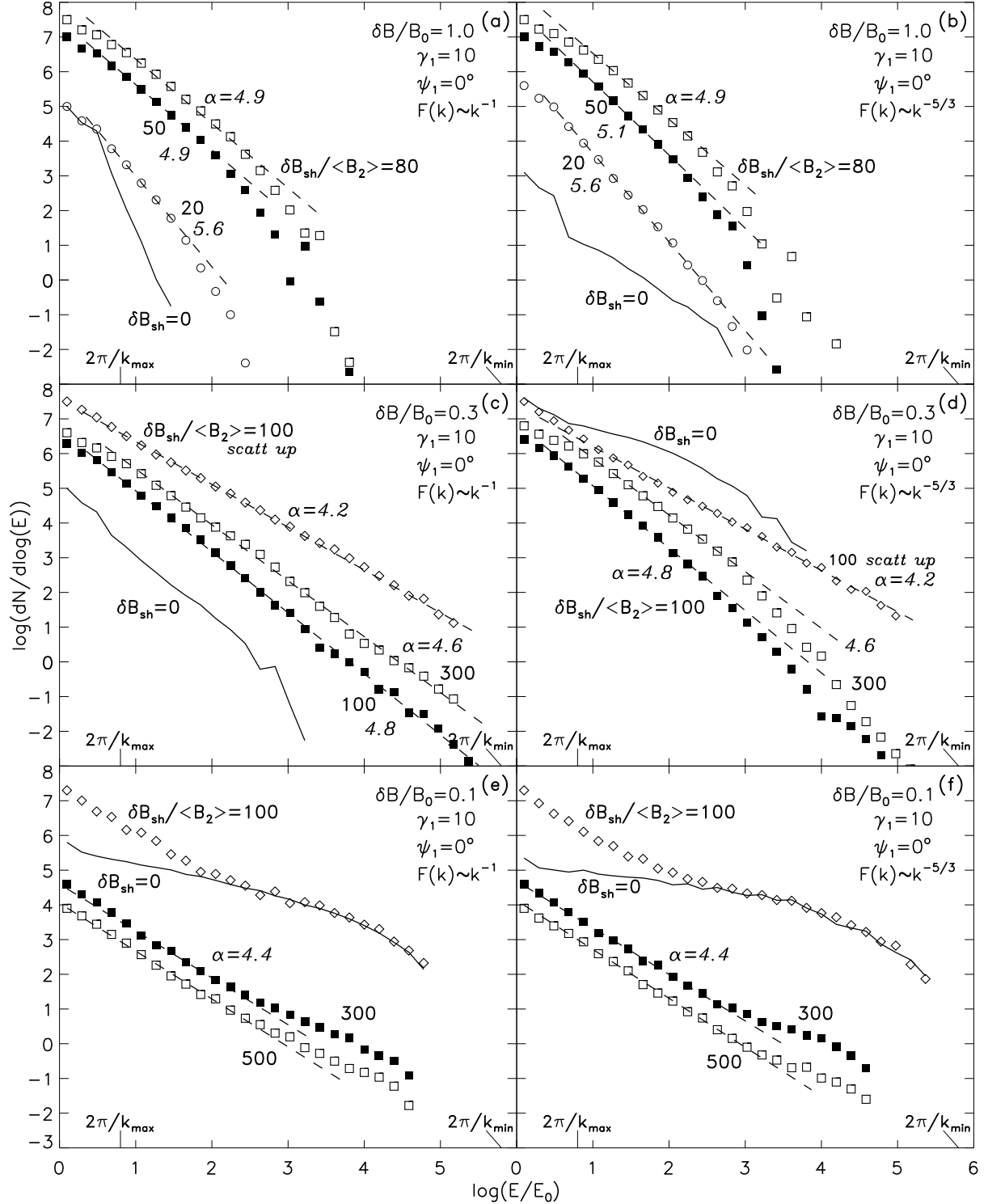


FIG. 6.— Accelerated particle spectra at parallel ultrarelativistic shocks ($\gamma_1 = 10, \psi_1 = 0^\circ$). The parameters of the large-scale background magnetic field turbulence structure are provided in each panel. The spectra shown with solid lines have been derived in simulations without small-scale perturbations (see Fig. 4 in Niemeic & Ostrowski 2006). The results indicated as “scatt up” in (c) and (d) show spectra obtained in simulations for which the particle pitch-angle diffusion was assumed to exist both downstream and upstream of the shock.

Figures 6a and 6b show the results for shocks with $\gamma_1 = 10$ and large-amplitude background field perturbations ($\delta B/B_0 = 1.0$). The qualitative similarity of the spectral features observed in this case and for oblique superluminal shocks is apparent (see also Niemeic & Ostrowski

2006)—the spectra are convex and display cutoffs occurring much below $E_{res,max} \simeq 2\pi/k_{min}$. This behavior proves that the large-amplitude long-wave perturbations locally form superluminal conditions at the shock, thus leading to a spectral cutoff as the pitch-angle scattering

term in the downstream shock-generated turbulence substantially decreases with growing particle energy. Note, that in the case of a lower amplitude of the short-wave component, $\delta B_{sh}/\langle B_2 \rangle = 20$, the large-scale background turbulence with Kolmogorov distribution provides additional particle scattering, allowing for the formation of a quasi-power-law spectrum in a slightly wider energy range than for the larger $\delta B_{sh}/\langle B_2 \rangle$ (Fig. 6b), again in correspondence to the analogous result for the superluminal shocks (Fig. 2).

For the smaller amplitude of the large-scale magnetic field perturbations, $\delta B/B_0 = 0.3$, the role of the long-wave perturbations is less significant and the scattering on the short-wave turbulence can dominate up to the energies higher than the upper resonance energy $E_{res,max}$. Though being gradually weaker with growing particle energy, in this case, as shown in Figure 6c, pitch-angle diffusion can dominate over scattering by the long-wave perturbations without a limit for particle energy below $E_{res,max}$. The scattering mean free paths along the mean background magnetic field (shock normal) and, correspondingly, the mean acceleration timescale also increase with particle energy, but the particle spectra retain a power-law form up to the highest energies $E \approx E_{res,max}$ studied in our simulations. However, the spectra are steeper than the expected “universal” spectrum, $\alpha > \alpha_u$, and only weakly dependent on δB_{sh} . To understand this feature, we have performed additional test simulations with the short-wave component introduced both downstream and *upstream* of the shock (with constant upstream scattering amplitude $\Delta\Omega(E)_{up} = const \ll 1/\gamma_1$). This case, equivalent to the pure pitch-angle diffusion model, should lead to the formation of the “universal” spectrum and, indeed, such the spectrum is produced in our simulations (described as “scatt up” in Fig. 6c). Thus, the slightly steeper spectra obtained in the models with only a downstream short-wave component can be understood solely as the result of the upstream long-wave turbulence providing a different distribution of pitch-angle perturbations to the particle orbits than the purely diffusive process (see Fig. 7). This allows for the generation of a power-law particle spectrum, but with somewhat steeper index than the “universal” value.

With the Kolmogorov background wave spectrum (Fig. 6d) there is enough power in long waves to influence the spectrum at high energies, leading to the noticeable steepening of the particle distributions below $E_{res,max}$. However, also in this case the model with the short-wave field perturbations imposed upstream of the shock yields the “universal” power-law spectrum. In Figure 7 we compare the angular distributions of particles at the shock in the cases of only downstream small-scale turbulence and with pitch-angle diffusion also upstream of the shock.

The spectra for weakly perturbed background magnetic fields, $\delta B/B_0 = 0.1$, presented in Figures 6e and 6f, show a new characteristic feature, namely a spectral bump besides the power-law spectrum at lower particle energies. The bump shape closely resembles the distribution of particles accelerated without the shock-generated field component (see the discussion in Niemiec & Ostrowski 2006), and its presence indicates that at these energies the short-wave perturbations become negligible compared to the background long-wave component. Note, that δB_{sh} is scaled with respect to

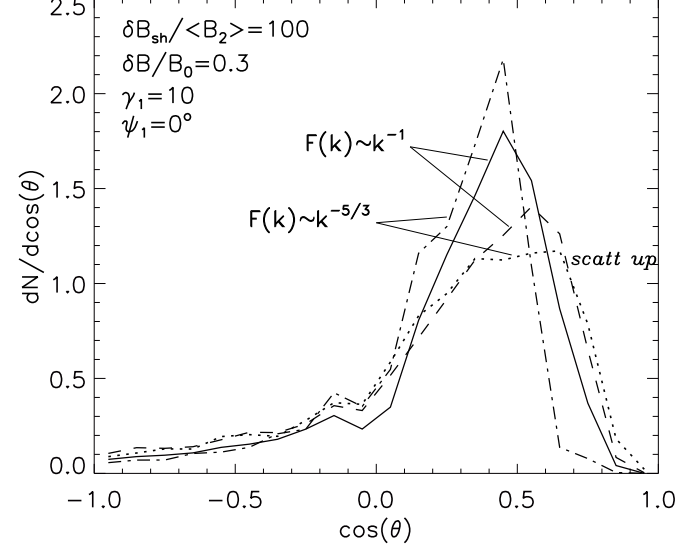


FIG. 7.— Particle angular distributions at parallel shocks ($\gamma_1 = 10$, $\psi_1 = 0^\circ$) for $\delta B_{sh}/\langle B_2 \rangle = 100$ and a weakly perturbed large-scale background magnetic field ($\delta B/B_0 = 0.3$) with either the flat (solid and dashed line) or the Kolmogorov (dash-dotted and dotted line) wave power spectrum of magnetic field perturbations. The distributions indicated as “scatt up” are derived in a model with short-wave turbulence imposed both downstream and upstream of the shock.

$\langle B_2 \rangle$, which is relatively small in comparison to the cases with larger $\delta B/B_0$ discussed above.

We have also performed a series of simulations for shocks with a larger Lorentz factor of $\gamma_1 = 30$. The particle spectra presented in Figure 8 for $\delta B_{sh}/\langle B_2 \rangle = 100$ show a similarity of spectral features to those observed for shocks with $\gamma_1 = 10$. However, there is an approximate scaling between the two cases, with characteristic spectral features appearing at respectively lower amplitudes of the long-wave magnetic field perturbations $\delta B/B_0$ for shocks with $\gamma_1 = 30$ than in the spectra for $\gamma_1 = 10$. Such a scaling may result from the stronger compression of these perturbations, as measured between the two plasma rest frames, and also from the larger particle anisotropy involved at the higher- γ shock.

4. CONCLUDING REMARKS

The present paper concludes our studies (Niemiec & Ostrowski 2004, 2006) of the first-order Fermi acceleration mechanism acting at relativistic and ultrarelativistic shock waves. We have attempted to consider as realistic models as possible for the perturbed magnetic field structures at the shock, which allow us to study all the field characteristics important for particle acceleration. In particular, we have investigated the dependence of particle spectra on the mean magnetic field inclination with respect to the shock normal and on the power spectra of magnetic field perturbations, including the long-wave background turbulence and the short-wave turbulence generated at the shock.

In the present paper we append the model of Niemiec & Ostrowski (2006) with downstream large-amplitude small-scale MHD turbulence component, analogous to those seen in PIC simulations of collisionless relativistic shocks. The form of these additional perturbations is arbitrarily chosen to consist of a very short

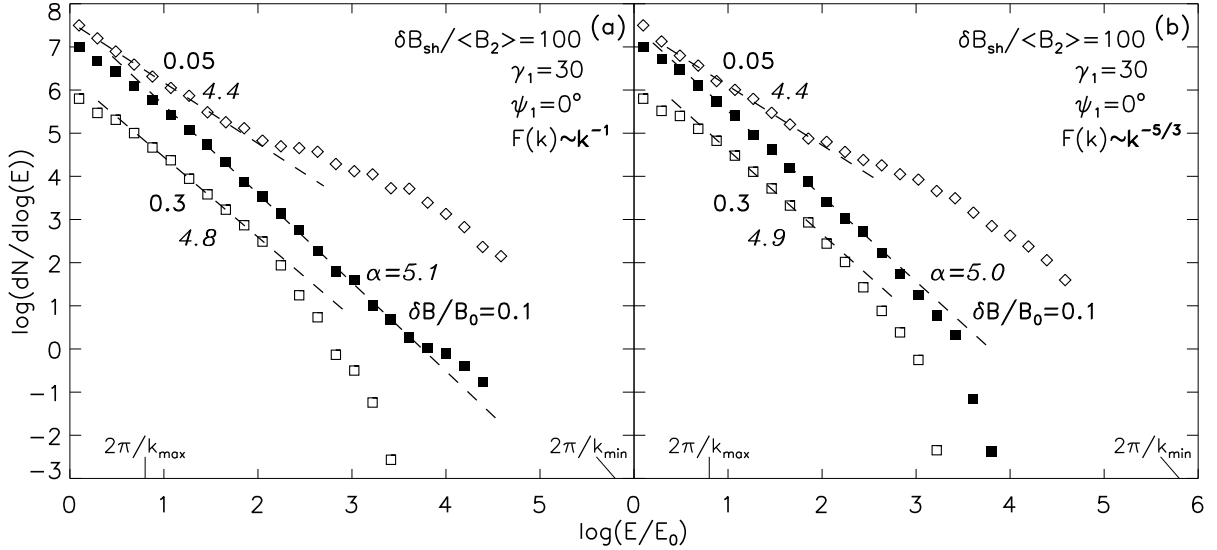


FIG. 8.— Particle spectra at parallel ($\psi_1 = 0^\circ$) ultrarelativistic shocks with $\gamma_1 = 30$, derived for a high amplitude of downstream short-wave perturbations $\delta B_{sh}/\langle B_2 \rangle = 100$, and (a) the flat and (b) the Kolmogorov wave-power spectrum of large-scale background magnetic field turbulence. The amplitudes of the background perturbations $\delta B/B_0$ are given near the respective results, together with the values of the spectral indices for fits to the power-law portions of the spectra.

sinusoidal waves, that form (static) isotropic highly nonlinear turbulence. We have considered a wide variety of ultrarelativistic shock configurations for which, as presented in §3, a number of different spectral features can be observed. We show that with growing particle energy the role of short-wave ($\lambda_{sh} \ll r_g(E)$) magnetic field perturbations decreases, and spectra at high energies are shaped only by the mean magnetic field and the long-wave perturbations. Thus, in oblique superluminal shocks concave particle spectra with cutoffs can be generated even for $\delta B_{sh} \gg \langle B_2 \rangle$. Extended power-law particle distributions can be formed in parallel shocks propagating in a medium with low-amplitude long-wave field perturbations, but the spectral indices obtained are larger than the “universal” spectral index $\alpha_u \approx 4.2$, that is widely considered in the literature. The only case in which we have been able to obtain spectra with $\alpha = \alpha_u$ involved the unphysical assumption, that large-amplitude short-wave field perturbations also exist upstream of the shock.

In summary, the accelerated particle spectral distributions obtained in this work and in our previous studies (Niemiec & Ostrowski 2004, 2006) generally differ from the spectra of relativistic electrons (power-laws with the spectral indices close to α_u) inferred from modeling the electromagnetic emission spectra of astrophysical sources hosting relativistic shocks (e.g., hot spots in extragalactic radio sources, quasar jets, gamma-ray burst afterglows). Our results thus provide a strong argument against considering the first-order Fermi shock acceleration as the main mechanism producing the observed radiating elec-

trons. In our opinion, other processes must be invoked to explain the observed emission spectra, for example second-order Fermi processes acting in the regions of relativistic MHD turbulence downstream of the shock, which have hardly ever been discussed for relativistic conditions till now (Virtanen & Vainio 2005), or the collisionless plasma processes that have been studied in numerous PIC simulations (e.g., Hoshino et al. 1992; Hedeland et al. 2004; Nishikawa et al. 2005b), or other non-standard acceleration processes like those discussed by Stern (2003) for electrons or Derishev et al. (2003) for both electrons and protons.

Our simulations also show, that relativistic shocks, being essentially always superluminal, possibly generate accelerated particle distributions with cutoffs below either the maximum resonance energy enabled by the *high-amplitude* background turbulence ($r_g(E_{cutoff}) < \lambda(E_{res,max})$), or approximately at the energy of the compressed background plasma ions $E_{cutoff} \sim \gamma_1 m_i c^2$ (where m_i is a mass of the heaviest ions present in the background medium). Thus, in conclusion, we maintain our opinion from the previous publications (see also Begelman & Kirk 1990) that relativistic shocks are not promising sites as possible sources of ultra-high-energy nuclei registered by the air shower experiments.

We are grateful to Mikhail Medvedev for interesting discussions. The present work was supported by MNiI in years 2005-2008 as a research project 1 P03D 003 29.

REFERENCES

Achterberg, A., Gallant, Y. A., Kirk, J. G., & Guthmann, A. W. 2001, MNRAS, 328, 393
 Bednarz, J., & Ostrowski, M. 1996, MNRAS, 283, 447
 Bednarz, J., & Ostrowski, M. 1998, Phys. Rev. Lett., 80, 3911
 Begelman, M. C., & Kirk, J. G. 1990, ApJ, 353, 66
 Derishev, E. V., Aharonian, F., Kocharyan, V. V., Kocharyan, Vl. V. 2003, Phys. Rev. D, 68, 043003
 Ellison, D. C., & Double, G. P. 2002, Astroparticle Phys., 18, 213
 Ellison, D. C., & Double, G. P. 2004, Astroparticle Phys., 22, 323

Frederiksen, J. T., Hededal, C., Haugbølle, T., & Nordlund, Å. 2004, *ApJ*, 608, L13

Gallant, Y. A., & Achterberg, A. 1999, *MNRAS*, 305, L6

Heavens, A., & Drury, L. O'C. 1988, *MNRAS*, 235, 997

Hededal, C., Haugbølle, T., Frederiksen, J. T., & Nordlund, Å. 2004, *ApJ*, 617, L107

Hededal, C., & Nishikawa, K.-I. 2005, *ApJ*, 623, L89

Hoshino, M., Arons, J., Gallant, Y. A., & Langdon, A. B. 1992, *ApJ*, 390, 454

Jaroschek, C. H., Lesch, H., & Treumann, R. A. 2005, *ApJ*, 618, 822

Keshet, U., & Waxman, E. 2005, *Phys. Rev. Lett.*, 94, 111102

Kirk, J. G., Guthmann, A. W., Gallant, Y. A., & Achterberg, A. 2000, *ApJ*, 542, 235

Kirk, J. G., & Heavens, A. 1989, *MNRAS*, 239, 995

Kirk, J. G., & Schneider, P. 1987, *ApJ*, 315, 425

Lemoine, M., & Pelletier, G. 2003, *ApJ*, 589, L73

Medvedev, M. V., & Loeb, A. 1999, *ApJ*, 526, 697

Niemiec, J., & Ostrowski, M. 2004, *ApJ*, 610, 851

Niemiec, J., & Ostrowski, M. 2006, *ApJ*, in press

Nishikawa, K.-I., Hardee, P., Richardson, G., Preece, R., Sol, H., & Fishman, G. J. 2003, *ApJ*, 595, 555

Nishikawa, K.-I., Hardee, P., Richardson, G., Preece, R., Sol, H., & Fishman, G. J. 2005, *ApJ*, 622, 927

Nishikawa, K.-I., Hardee, P., Hededal, C., & Fishman, G. J. 2005, *ApJ*, accepted

Ostrowski, M. 1991, *MNRAS*, 249, 551

Ostrowski, M. 1993, *MNRAS*, 264, 248

Ostrowski, M., & Bednarz, J. 2002, *A&A*, 394, 1141

Silva, L. O., Fonseca, R. A., Tonge, J. W., Dawson, J. M., Mori, W. B., & M. Medvedev, M. V. 2003, *ApJ*, 596, L121

Stern, B.E. 2003, *MNRAS*, 345, 590

Virtanen, J., & Vainio, R. 2005, *ApJ*, 621, 313